ANFIS-Based State Observer for a Feedback Inverted Pendulum: Experimental Validation

Javiera Miranda-Ordenes[1], Lisbel Bárzaga-Martell[1], Norelys Aguila-Camacho[2], and Guillermo González-Romero[3]

***Abstract*— The inverted pendulum is a benchmark system for evaluating estimation and control strategies due to its strong nonlinearity, inherent instability, and sensitivity to noise and modeling uncertainties. Although adaptive neuro-fuzzy inference systems (ANFIS) have been widely employed as controllers or predictors, their use as state observers under real experimental conditions remains limited. This paper presents an ANFIS-based observer for estimating unmeasured velocity states of a cart–inverted pendulum system, with particular emphasis on the reconstruction of the pendulum angular velocity for feedback control. The proposed observer is experimentally evaluated and compared with a model-based Extended Kalman Filter (EKF) under identical operating conditions within a switched angle–position control architecture. Estimated velocities are incorporated into the swing-up control logic as an alternative to classical numerical differentiation of encoder signals. Experimental results indicate that, while numerical differentiation provides a straightforward velocity approximation, observer-based approaches offer enhanced robustness to measurement noise and transient dynamics. In particular, the ANFIS observer yields smoother short-term velocity estimates during the swing-up phase, whereas the EKF exhibits favorable long-term estimation consistency. Both observers lead to comparable control effort in closed-loop operation. Overall, the results demonstrate that EKF- and ANFIS-based observers constitute robust alternatives to numerical differentiation for experimental nonlinear control applications, especially in scenarios characterized by strong nonlinearities, measurement noise, and limited model accuracy.**

I. INTRODUCTION

The inverted pendulum on a cart system has become one of the most widely used experimental platforms for validating advanced control techniques, owing to its inherently nonlinear, underactuated, and open-loop unstable dynamics [1]. The system is characterized by a single control input—the force applied to the cart—and two measurable outputs: the cart's linear position and the pendulum's angular displacement with respect to the vertical. Its dynamic behavior exhibits strong similarities with a broad class of real-world systems, including robotic manipulators, self-balancing vehicles, aerospace platforms, and bipedal robots [2]. These features have established the inverted pendulum as a benchmark problem in both academic and control-oriented research, serving as a representative testbed for the development, analysis, and experimental validation of modern control strategies [3].

From an automatic control perspective, the primary objective is to stabilize the pendulum around the upright vertical equilibrium after lifting it from its natural resting configuration, while simultaneously ensuring fast and accurate regulation of the cart position. Conventionally, this problem is addressed by linearizing the nonlinear dynamics about the unstable equilibrium point, thereby enabling the systematic application of classical control techniques such as PID [4] and advanced strategies including Linear Quadratic Regulators (LQR) and Model Predictive Control (MPC) [5].

The swing-up and stabilization phases inherently require velocity-related state variables, particularly the pendulum's angular velocity and the cart's translational velocity. In most practical implementations of the inverted pendulum, these states are not directly measurable. A straightforward mathematical approach is to obtain them by differentiating the measured angular and cart position signals; however, numerical differentiation significantly amplifies measurement noise, degrading closed-loop performance and reducing robustness. To overcome this limitation, nonlinear state observers, such as the Extended Kalman Filter (EKF), are commonly employed [6], as they enable reliable estimation of unmeasured states while explicitly accounting for system nonlinearities and measurement noise.

Nevertheless, the use of the EKF is not entirely optimal, since it relies on an accurate mathematical model of the inverted pendulum. In practice, this requirement is difficult to satisfy due to parametric uncertainties, unmodeled dynamics, friction effects, and variations in system parameters, which are typical of experimental platforms. As an alternative to model-based state observers, model-free estimation approaches have gained increasing attention. These estimators do not depend explicitly on a precise system model; instead, they use available measurements to infer the system states. Among the techniques particularly relevant to control applications are schemes based on fuzzy logic and neuro-fuzzy systems [7], as well as advanced intelligent control strategies such as super-twisting control [8], which offer enhanced robustness against uncertainties and modeling errors.

In the context of sensorless state estimation, Senthil *et al.* [9] propose a hybrid observer framework in which ANFIS

*This work was supported by ANID-FONDECYT 3240317 and 1220168

[1]Javiera Miranda-Ordenes and Lisbel Bárzaga Martell are with Departamento de Electricidad, Universidad Tecnológica Metropolitana, Av. José Pedro Alessandri 1242, Santiago 7800002, Chile. lisbel.barzaga@utem.cl

[2] Norelys Aguila-Camacho is with School of Engineering, University of North Florida, 1 UNF Drive Jacksonville, FL 32224, United States of America norelys.aguila.camacho@unf.edu

[3]Guillermo González-Romero is with Departamento de Ingeniería Eléctrica, Universidad de Santiago de Chile (USACH), Av. Victor Jara 3519, Santiago 9170124, Chile. guillermo.gonzalez.r@usach.cl

is employed to enhance the accuracy and robustness of rotor position and speed estimation in a switched-reluctance motor drive. In their approach, classic sliding-mode observers are combined with intelligent adaptation mechanisms, in which ANFIS is employed to minimize estimation errors and dynamically adjust observer gains across different operating regions. Rather than relying exclusively on precise machine parameters, the ANFIS-based structure learns the nonlinear relationship between measurable electrical quantities and unmeasured mechanical states, thereby reducing sensitivity to parameter variations, noise, and changes in operating point. This work illustrates how ANFIS can be effectively integrated within observer architectures, reinforcing its suitability as a model-free observer for nonlinear systems.

Unlike most existing work, which primarily employs ANFIS as a controller or an auxiliary tuning mechanism, this study explicitly uses ANFIS as a standalone nonlinear state observer for the inverted pendulum system. Furthermore, the proposed approach is experimentally validated within a complete swing-up and stabilization framework and benchmarked against a model-based EKF observer, highlighting its effectiveness under practical uncertainties.

The remainder of this paper is organized as follows. Section II presents the mathematical model of the inverted pendulum system, together with the proposed ANFIS observer–controller design. Section III reports the experimental results and provides a detailed discussion and analysis of the obtained outcomes. Finally, Section IV summarizes the main conclusions of the study.

II. System Modeling and ANFIS Observer–Controller Design

Figure 1 presents the complete block diagram of the proposed control and state estimation framework for the inverted pendulum–cart system. The architecture integrates a switched control strategy with an ANFIS-based state observer. The control scheme consists of a swing-up and stabilization controller and a lower-zone stabilization and crane controller, whose outputs are selected through a switching mechanism to generate the control input u_k applied to the plant. The inverted pendulum system provides two measurable outputs: the cart position x_k and the pendulum angle θ_k, which are fed back to the observer structure. Within the estimation layer, the ANFIS observer estimates the unmeasured states through a multi-layer neuro-fuzzy inference process driven by the measured signals and the control input. Finally, the estimated angular velocity is fed back to the controller, completing the closed-loop architecture. The subsequent subsections detail the individual schemes.

A. Inverted Pendulum–cart Mathematical Model

The experimental validation is conducted on the inverted pendulum–cart platform Unit 33-200, manufactured by Feedback Instruments Ltd. [10], which is installed in the research group's laboratory. The setup consists of a mechanical inverted pendulum–cart assembly driven by a DC motor, an interface module, and a communication unit that allows real-time interaction with a host computer running MATLAB. Signal acquisition and actuation are handled through an Advantech PCI-1711U-CE data acquisition card, which interfaces the sensors and actuators with the control algorithms.

The cart motion is generated by a DC motor whose electromechanical behavior is described by the following dynamics:

$$J\dot{\omega}(t) = K_t i(t) - B\omega(t), \tag{1}$$

$$L\dot{i}(t) = v(t) - Ri(t) - K_b\omega(t), \tag{2}$$

where $i(t)$ denotes the armature current, $v(t)$ the applied voltage, and $\omega(t)$ the motor angular velocity. The parameters J, B, K_t, and K_b correspond to the rotor inertia, viscous friction coefficient, torque constant, and back electromotive force constant, respectively, while R and L represent the armature resistance and inductance.

The interaction between the DC motor and the cart–pendulum mechanism is modeled by relating the control force F acting on the cart to the motor current according to

$$F = -k_F 600 K_t i(t), \tag{3}$$

as specified by the manufacturer's simulation environment [10]. Under this configuration, the actuator is capable of delivering forces up to ± 20 N for input voltages within ± 2.5 V.

The nonlinear dynamics of the inverted pendulum–cart system are described by the coupled equations [4]:

$$(M+m)\ddot{x} + b\dot{x} + ml\ddot{\theta}\cos\theta - ml\dot{\theta}^2\sin\theta = F, \tag{4}$$

$$(I+ml^2)\ddot{\theta} - mgl\sin\theta + ml\ddot{x}\cos\theta + d\dot{\theta} = 0, \tag{5}$$

where x denotes the cart position and θ the pendulum angle measured from the vertical. The parameters M and m correspond to the masses of the cart and pendulum, respectively; l is the pendulum length; I is its moment of inertia; b and d represent viscous friction coefficients associated with the cart and pendulum; and g is the gravitational acceleration. The physical parameters of the DC motor and the inverted pendulum correspond to those reported in [4] (Table 1).

By discretizing the continuous-time dynamics using a forward Euler scheme, the system can be represented in discrete-time state-space form as:

$$\mathbf{x}_k = \mathbf{A}\mathbf{x}_{k-1} + \mathbf{B}\mathbf{u}_k, \tag{6}$$

$$\mathbf{y}_k = \mathbf{C}\mathbf{x}_k, \tag{7}$$

where the state vector $\mathbf{x}_k \in \mathbb{R}^6$ collects the mechanical and electrical states of the coupled system, namely, $\mathbf{x}_k = [x,\ \dot{x},\ \theta,\ \dot{\theta},\ i,\ \omega]^T$.

The linearized discrete-time model in (6) is obtained around the unstable equilibrium point $\theta = 0$. Under this approximation, the closed-loop system governed by the controllers defined in the next section satisfies standard linear stability conditions in the vicinity of the upright configuration. The control input $\mathbf{u}_k = F$ corresponds to the force applied to the cart, while the output vector $\mathbf{y}_k$ comprises

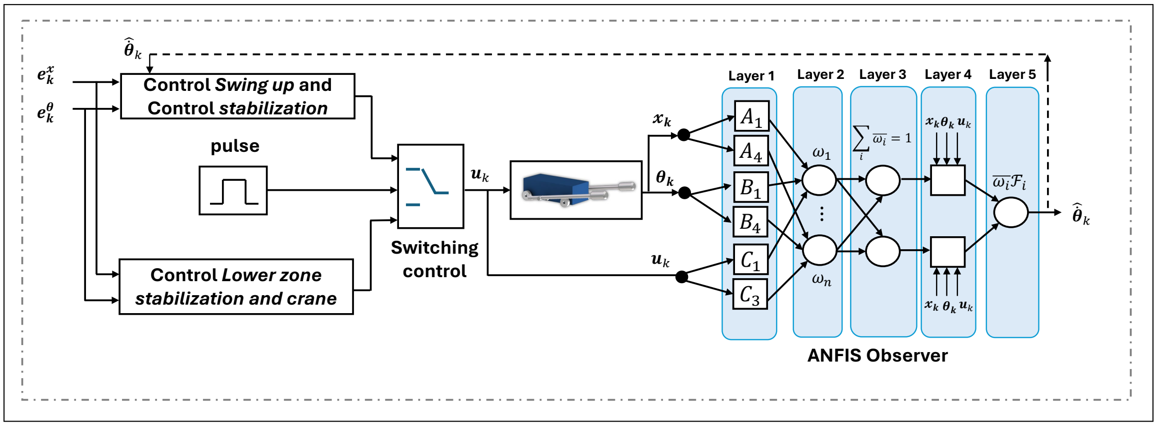

Fig. 1. Block diagram for estimation and control in the car–inverted pendulum system.

the measurable cart position x and pendulum angle θ. The matrices $\mathbf{A} \in \mathbb{R}^{6\times6}$, $\mathbf{B} \in \mathbb{R}^{6\times1}$, and $\mathbf{C} \in \mathbb{R}^{2\times6}$ are defined as

$$\mathbf{A} = \frac{1}{\alpha}\begin{bmatrix} 0 & \alpha & 0 & 0 & 0 & 0 \\ 0 & -a_1 & -a_2 & a_3 & a_4 & 0 \\ 0 & 0 & 0 & \alpha & 0 & 0 \\ 0 & a_5 & a_6 & -a_7 & -a_8 & 0 \\ 0 & 0 & 0 & 0 & -\alpha R/L & -\alpha K_b/L \\ 0 & 0 & 0 & 0 & \alpha K_t/J & -\alpha B/J \end{bmatrix}, \tag{8}$$

$$\mathbf{B} = \begin{bmatrix} 0 & 0 & 0 & 0 & 1/L & 0 \end{bmatrix}^T, \quad \mathbf{C}^T = \begin{bmatrix} 1 & 0 \\ 0 & 0 \\ 0 & 1 \\ 0 & 0 \\ 0 & 0 \\ 0 & 0 \end{bmatrix}, \tag{9}$$

with $\alpha = (M+m)(I+ml^2) - (ml)^2$, and coefficients a_i defined according to the physical parameters of the system [4].

B. Switched Angle–Position Control Scheme

The control strategy adopted in this work is based on a switched angle-position scheme composed of three main controllers: a swing-up controller, a stabilization controller, and a fall-crane controller. These controllers operate sequentially according to the pendulum angular position and are coordinated through a hybrid switching mechanism, enabling full rotational maneuverability of the pendulum while ensuring robust stabilization around the upright equilibrium.

During the swing-up phase, the total control input applied to the cart-pendulum system is expressed as the superposition of a nonlinear swing-up voltage, an initialization pulse, and an auxiliary cart position regulation term. The main swing-up component is generated through a smooth nonlinear function of the pendulum angle, which allows gradual energy injection during both the initial and final stages of the maneuver.

The direction of the applied voltage is determined by a logic-based sign switching mechanism that depends on the pendulum angular velocity and its position relative to predefined upper and lower angular zones. This strategy ensures that energy is injected in phase with the pendulum motion, thereby avoiding undesired braking effects.

During the swing-up phase, the control input applied to the cart-pendulum system is defined as

$$u_k = u_{\mathrm{su}} + u_{\mathrm{c}} + u_{\mathrm{f}}, \tag{10}$$

where u_{su} is the nonlinear swing-up term, u_{c} is an auxiliary *PI* controller acting on the cart position during swing-up, and u_{f} is a short initialization pulse. The swing-up term is generated through an angle-dependent nonlinear function,

$$u_{\mathrm{raw}}(t) = 0.2\sin\big(\theta(t)\big)\,\big|\sin\big(\theta(t)\big)\big|, \tag{11}$$

whose sign is switched according to the angular velocity of the pendulum and its position relative to predefined upper and lower angular zones,

$$u_{\mathrm{su}}(t) = \sigma(t)\,u_{\mathrm{raw}}(t), \qquad \sigma(t) \in \{-1,\, 1\}. \tag{12}$$

The sign function $\sigma(t)$ explicitly depends on the estimated angular velocity $\hat{\dot{\theta}}_k$, provided either by the ANFIS-based observer or the EKF.

$$\sigma(t) = \begin{cases} +1, & \hat{\dot{\theta}}(t) \geq 0\ , \\ -1, & \hat{\dot{\theta}}(t) < 0\ . \end{cases} \tag{13}$$

Finally, a short-duration pulse $u_{\mathrm{f}}(t)$ is applied at startup to overcome static friction and guaranty the onset of oscillatory motion.

$$u_{\mathrm{f}}(t) = \begin{cases} 0.4, & 0 \leq t \leq 0.3 \text{ s}, \\ 0, & t > 0.3 \text{ s}. \end{cases} \tag{14}$$

The swing-up controller is disabled once the pendulum enters a small neighborhood of the upright equilibrium, at which point the stabilization controller is activated. The transition to the stabilization phase is carried out as follows:

$$u_k = \begin{cases} u_{\mathrm{stab}}, & \text{if } |\hat{\dot{\theta}}_k| \leq \varepsilon \ \wedge\ |\theta_k| \leq \theta_c, \\ u_{\mathrm{su}}, & \text{otherwise}, \end{cases} \tag{15}$$

where ε and θ_c define a capture region around the upright equilibrium. The velocity threshold ε is adaptively defined as

$$\varepsilon = \begin{cases} \varepsilon_0, & \text{if } \theta_k \leq \dfrac{\pi}{2} \text{ or } \theta_k \geq \dfrac{3\pi}{2}, \\ 0, & \text{otherwise,} \end{cases} \tag{16}$$

where ε_0 is a small positive constant set to 0.5 rad/s. This angular condition restricts voltage inversion to the upper region of the pendulum motion, preventing unnecessary switching during large-amplitude oscillations and ensuring effective energy injection during the swing-up phase. The stabilization and fall-crane controllers are defined as combinations of two PID controllers:

$$\begin{cases} u_{\text{stab}} = \text{PID}_1 - \text{PID}_2, \\ u_{\text{fall-crane}} = \text{PID}_3 - \text{PID}_4. \end{cases} \tag{17}$$

Here, PID_1 and PID_3 correspond to the cart position controllers, while PID_2 and PID_4 regulate the pendulum angle. Each PID subcontroller follows a standard structure with filtered derivative action to attenuate high-frequency noise, given by the following transfer function:

$$\text{PID}_i(s) = K_{P_i} + \frac{K_{I_i}}{s} + K_{D_i} f_\Delta, \quad i = 1, \ldots, 4, \tag{18}$$

where the derivative filter is given by

$$f_\Delta(s) = \frac{10^3}{s^2 + 70.7s + 10^3}.$$

The control scheme considers two tracking error signals associated with the cart position and the pendulum angle. The cart position tracking error, which is used as the input to PID1 and PID3, is defined as $e_k^x = x_k - r_x$, whereas the pendulum angle tracking error, which is fed to PID2 and PID4, is defined as $e_k^\theta = \theta_k - r_\theta$. Similarly, the estimation error for the pendulum velocity is defined as $e_k^{\hat{\dot\theta}} = \dot\theta_k - \hat{\dot\theta}_k$.

C. ANFIS-Based State Observer

In order to estimate the unmeasured pendulum angular velocity required by the switched angle–position control scheme (15), an Adaptive Neuro-Fuzzy Inference System (ANFIS) is employed as a nonlinear model-free state observer. To avoid noise amplification associated with numerical differentiation, the proposed observer reconstructs $\dot\theta$ directly from the measured cart position x, pendulum angle θ, and the applied control input $\mathbf{u}_k$.

The ANFIS observer is formulated as a nonlinear mapping between the measured signals and the unmeasured angular velocity and is defined as

$$\hat{\dot\theta}_{k+1} = \mathcal{F}(\mathbf{v}_k), \tag{19}$$

where $\hat{\dot\theta}_k$ denotes the estimated pendulum angular velocity.

The input vector to the ANFIS observer is given by $\mathbf{v}_k = [x_k, ; \theta_k, ; u_k]^T$, which comprises the measured cart position, the measured pendulum angle, and the applied control input. The nonlinear mapping $\mathcal{F}(\cdot)$ is implemented through a fixed-rule Takagi–Sugeno neuro-fuzzy structure and provides one-step-ahead estimates of the unmeasured pendulum angular velocity.

The ANFIS-based observer implemented in this work follows a fixed-rule Takagi–Sugeno architecture (Fig. 1), which is described in the following paragraphs.

Layer 1: Fuzzification Layer: In the first layer, each node computes the membership degree of the ANFIS input variables. The input vector is defined as

$$\mathbf{v}_k = \begin{bmatrix} x_k & \theta_k & u_k \end{bmatrix}^T. \tag{20}$$

Each input variable $v_{j,k}$, $j = 1, 2, 3$, is associated with a predefined set of membership functions obtained via grid partition. The output of the i-th node in the fuzzification layer corresponding to the j-th input is given by

$$O_{i,j}^{(1)} = \mu_{A_{i,j}}(v_{j,k}), \tag{21}$$

where $\mu_{A_{i,j}}(\cdot)$ denotes the membership function of the fuzzy set $A_{i,j}$.

In this work, generalized bell-shaped membership functions are employed,

$$\mu_{A_{i,j}}(v_{j,k}) = \frac{1}{1 + \left| \frac{v_{j,k} - c_{i,j}}{a_{i,j}} \right|^{2b_{i,j}}}, \tag{22}$$

where $(a_{i,j}, b_{i,j}, c_{i,j})$ are the premise parameters. The input variables x_k, θ_k, and u_k are mapped into 4, 4, and 3 fuzzy sets, respectively, yielding a total of 48 fuzzy rules.

Layer 2: Rule Layer: Each node in the second layer represents a fuzzy rule and computes its firing strength by aggregating the membership degrees of the corresponding inputs. Given the fixed-rule Takagi-Sugeno structure, the firing strength of the i-th rule is computed as

$$O_i^{(2)} = \omega_i = \prod_{j=1}^{3} \mu_{A_{i,j}}(v_{j,k}), \quad i = 1, \ldots, N_r, \tag{23}$$

where $N_r = 48$ denotes the total number of fuzzy rules.

Layer 3: Normalization Layer: In the third layer, the firing strengths are normalized to ensure balanced rule contribution. The normalized firing strength of the i-th rule is given by

$$O_i^{(3)} = \bar\omega_i = \frac{\omega_i}{\sum_{r=1}^{N_r} \omega_r}, \quad i = 1, \ldots, N_r. \tag{24}$$

Layer 4: Consequent Layer: In the fourth layer, each fuzzy rule generates a linear consequent of the form

$$F_i = a_{i1} x_k + a_{i2} \theta_k + a_{i3} u_k + b_i, \quad i = 1, \ldots, N_r, \tag{25}$$

where a_{ij} and b_i are the consequent parameters associated with the i-th fuzzy rule.

Layer 5: Output Layer: Finally, in the fifth layer, the ANFIS output $\mathcal{F}$ is obtained as a weighted sum of the rule consequents,

$$\mathcal{F} = \sum_{i=1}^{N_r} \bar\omega_i F_i. \tag{26}$$

In the proposed observer configuration, the output $\mathcal{F}$ corresponds to the estimated pendulum angular velocity $\hat{\dot\theta}_k$, which is fed back into the switched control scheme to support the swing-up phase.

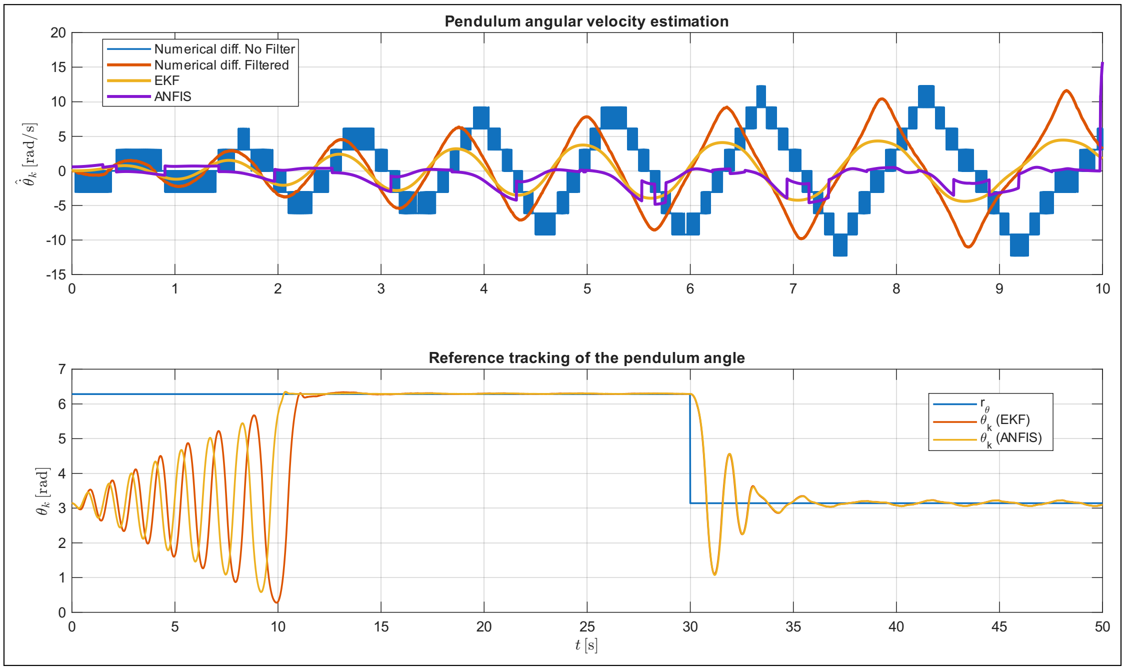

Fig. 2. Experimental results: (top) pendulum angular velocity estimation using EKF, ANFIS, and numerical differentiation, filtered and unfiltered; (bottom) reference tracking of the pendulum angle.

The parameters of the ANFIS observer, including the premise parameters of the generalized bell membership functions and the linear consequent parameters, are trained offline using experimental data collected from the inverted pendulum system under representative operating conditions. The training dataset consists of 18 independent experimental runs covering three regimes: (i) cart position control only, (ii) simultaneous cart-pendulum regulation around the stable equilibrium ($\theta = \pi$), and (iii) swing-up and stabilization around the inverted equilibrium ($\theta = 0$), capturing both transient and steady-state behaviors.

To prevent data leakage, the trained ANFIS observer is validated and evaluated online using experimental runs not included in the training set. Once trained, the observer operates in real time and provides smooth and noise-robust estimates of the pendulum angular velocity, which are directly supplied to the switched angle-position controller shown in Fig. 1.

In the subsequent section, the performance of the proposed ANFIS-based observer is experimentally evaluated and compared against a model-based Extended Kalman Filter, which is included as a benchmark estimator to assess the relative performance of the proposed approach.

III. Experimental Results and Performance Analysis

All numerical simulations were carried out using MATLAB® 2025, while the experimental implementation was executed in MATLAB® 2017. The ANFIS models were trained on a desktop computer equipped with an Intel Core i9-12900KF processor, 64 GB of DDR4 RAM, and an NVIDIA GeForce RTX 3090 graphics card with 24 GB of memory. Each experiment was run over time horizons of 10 s and 50 s, with a constant sampling period of $T_s = 0.001$ s.

TABLE I

PID and PI controller gains employed in the switched control scheme [4].

Gain	PID_1	PID_3	PID_2	PID_4	PI
K_P	7	25	7	4	0.5
K_I	0.5	0.2	2	0	0.2
K_D	3	2	1	0.1	–

TABLE II

Performance indices for EKF and ANFIS observers computed over the first 10 s (swing-up phase).

Obs.	RMSE ($e_k^{\dot{\theta}}$)	IAE ($e_k^{\dot{\theta}}$)	ISU ($\mathbf{u}_k$)
EKF	4.3932	**19.2159**	1.17714
ANFIS	**2.4898**	34.8032	**1.12817**

For the EKF parameters, the initial estimated state was generated as $\hat{\mathbf{x}}_0 \sim \mathcal{N}\left(\mathbf{x}_0, 0.01^2\mathbf{I}_6\right)$, with $\mathbf{x}_0 = [0,\ 0,\ 0.01,\ 0,\ 0,\ 0]^T$. Subsequently, the EKF tuning was completed by selecting the process and measurement noise covariance matrices as $\mathbf{Q} = 0.1\mathbf{I}_6$ and $\mathbf{R} = 0.01\mathbf{I}_2$, respectively, where $\mathbf{I}_n$ denotes the $n \times n$ identity matrix. The initial estimation error covariance matrix was set as $\mathbf{P} = \mathrm{diag}(\hat{\mathbf{x}}_0)$. These initial and tuning parameters were chosen in accordance with standard EKF design guidelines reported in the literature [4], [10].

The gains of the PID and PI controllers employed within the switched control architecture are summarized in Table I.

Figure 2 presents the experimental pendulum angular velocity estimation obtained using the EKF, the ANFIS-based observer, and numerical differentiation, both filtered and unfiltered, together with the pendulum angle reference tracking. Table II reports the performance indices computed over the first 10 s of operation, corresponding to the swing-up phase, during which the estimated angular velocity $\hat{\dot{\theta}}_k$ directly affects the control input.

Under these conditions, the ANFIS-based observer achieves lower RMSE values for the pendulum angular velocity estimation, reducing the RMSE from 4.39 (EKF) to 2.48 (ANFIS), while the IAE increases from 19.21 to 34.80, the latter due to the EKF estimation being closer to the numerical differentiation signal (see Fig. 2), which is the one used to calculate estimation errors. Still, the most important aspect is that once the pendulum enters the capture region, both estimation schemes enable accurate reference tracking during the stabilization phase, with no sustained oscillations, indicating that the estimated velocity signals are sufficiently reliable to support the switching logic and closed-loop control action. Moreover, it can be observed from Fig. 2 (bottom plot) that the controller operating with ANFIS gets the pendulum to the stabilization zone faster than the controller with EKF.

From a control standpoint (Figure 3), both observers lead to comparable control efforts. The ANFIS-based implementation yields a slightly lower ISU (1.12) than the EKF-based scheme (1.17), suggesting that improved short-term velocity estimation during the swing-up phase can result in a modest reduction in input energy.

Although the pendulum angular velocity can, in principle, be obtained by numerical differentiation of the encoder signal, this approach strongly amplifies measurement noise and encoder quantization, producing pronounced high-frequency oscillations (Figure 2 - blue signal), particularly during the swing-up phase. In practice, a differentiator therefore requires additional low-pass filtering to yield a usable velocity signal (Figure 2 - orange signal). In contrast, EKF- and ANFIS-based observers exploit either model-based dynamics or data-driven nonlinear mappings to provide inherent noise attenuation and improved robustness to unmodeled dynamics and disturbances, enabling more reliable velocity estimates for control and performance evaluation.

Overall, while the EKF provides accurate estimation when a reliable model is available, the ANFIS observer constitutes a competitive model-free alternative, exhibiting comparable experimental performance without relying on explicit system dynamics. Although the experimental validation in this work is conducted on an inverted pendulum platform, the use of data-driven, model-free observers can naturally be extended to robotic manipulators and mechanical systems with higher degrees of freedom, where nonlinearities, modeling uncertainties, and reliable velocity estimation remain significant challenges.

IV. CONCLUSIONS

This work experimentally compared velocity estimation strategies for a cart–inverted pendulum system using an EKF, an ANFIS-based observer, and numerical differentiation of encoder measurements. While numerical differentiation provides a simple approximation, observer-based methods are more robust under noisy, transient conditions. The ANFIS observer provided improved short-term estimation during swing-up with control effort comparable to the EKF, whereas the EKF exhibited more consistent long-term behavior. Overall, both observers represent robust alternatives to numerical differentiation for experimental nonlinear control applications.

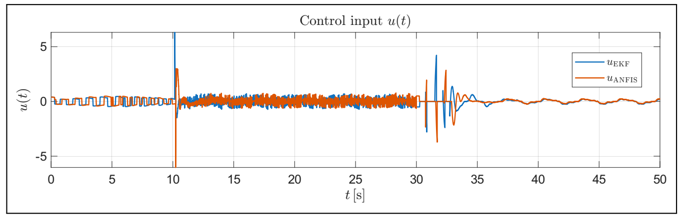

Fig. 3. Control input under swing-up and stabilization: EKF (blue) and ANFIS (orange).

ACKNOWLEDGMENT

ANID-FONDECYT partly supported this work under grant number 3240317 and 1220168.

REFERENCES

[1] T. T. Sarkar, L. Dewan, and C. Mahanta, “Real time swing up and stabilization of rotary inverted pendulum system,” in *2020 International conference on computational performance evaluation (ComPE)*. IEEE, 2020, pp. 517–522.

[2] O. Gonzalez and A. Rossiter, “Fast hybrid dual mode nmpc for a parallel double inverted pendulum with experimental validation,” *IET Control Theory & Applications*, vol. 14, no. 16, pp. 2329–2338, 2020.

[3] S. P. Diwan and S. S. Deshpande, “A hybrid optimizer based nonlinear model predictive control for rotary inverted pendulum,” in *2022 International Conference on Automation, Computing and Renewable Systems (ICACRS)*. IEEE, 2022, pp. 121–127.

[4] M. Fernández-Jorquera, M. Zepeda-Rabanal, N. Aguila-Camacho, and L. Bárzaga-Martell, “Design, tuning, and experimental validation of switched fractional-order pid controllers for an inverted pendulum system,” *Fractal and Fractional*, vol. 9, no. 4, 2025.

[5] E. S. Varghese, A. K. Vincent, and V. Bagyaveereswaran, “Optimal control of inverted pendulum system using pid controller, lqr and mpc,” in *IOP Conference Series: Materials Science and Engineering*, vol. 263. IOP Publishing, 2017, p. 052007.

[6] S. Hoseini and J. Poshtan, “Fault tolerant control applied on an inverted pendulum by using extended kalman filter,” in *2007 International Conference on Intelligent and Advanced Systems*. IEEE, 2007, pp. 945–948.

[7] J. A. Pucheta, C. R. Rivero, S. O. Laboret, C. A. Salas, and M. Herrera, “Stability analysis of the neurocontroller-observer for a inverted pendulum case,” in *2017 XVII Workshop on Information Processing and Control (RPIC)*. IEEE, 2017, pp. 1–6.

[8] Q. Pan, J. Fei, and Y. Xue, “Adaptive intelligent super-twisting control of dynamic system,” *IEEE Access*, vol. 10, pp. 42 396–42 403, 2022.

[9] L. Senthil Murugan and P. Maruthupandi, “Sensorless speed control of 6/4-pole switched reluctance motor with anfis and fuzzy-pid-based hybrid observer,” *Electrical Engineering*, vol. 102, no. 3, pp. 1527–1545, 2020.

[10] *Digital Pendulum Control Experiments, Manual: 33-936S, Feedback Instruments Ltd.*